

Available at www.sciencedirect.comjournal homepage: www.elsevier.com/locate/issn/15375110

Research Paper

Robust climate control of a greenhouse equipped with variable-speed fans and a variable-pressure fogging system

Raphael Linker^{a,*}, Murat Kacira^b, Avraham Arbel^c

^a Division of Environmental, Water and Agricultural Engineering, Faculty of Civil and Environmental Engineering, Technion – Israel Institute of Technology, Haifa 32000, Israel

^b Agricultural and Biosystems Engineering, University of Arizona, Tucson, AZ 85721, USA

^c Institute of Agricultural Engineering, Agricultural Research Organization, The Volcani Center, Bet-Dagan 50250, Israel

ARTICLE INFO

Article history:

Received 28 March 2011

Received in revised form

14 July 2011

Accepted 25 July 2011

Published online 31 August 2011

A climate control system for a small greenhouse equipped with a variable-pressure fogging system and variable-speed extracting fans was developed and validated. The controllers were designed using the robust control method quantitative feedback theory (QFT) that guarantees adequate performance of the controlled system despite large modelling uncertainties and disturbances. In order to simplify the design of the controllers and achieve better performances, partial decoupling between the two control loops was achieved by describing the greenhouse climate in terms of air enthalpy and humidity ratio. This led to using ventilation for achieving the desired air enthalpy, and fogging for achieving the desired humidity ratio, assuming that the ventilation rate was approximately known. The implementation results demonstrated the good performance of the controllers, with mean tracking errors of $\sim 100 \text{ J kg}^{-1}$ [dry air] and $\sim 0.1 \text{ g [water] kg}^{-1}$ [dry air] for enthalpy and humidity ratio, respectively. For practical applications, the desired climate was expressed in terms of air temperature and relative humidity, which were converted into enthalpy and humidity ratio using the psychrometric relationships. In this case, the mean tracking errors were $\sim 0.2 \text{ }^\circ\text{C}$ air temperature and less than 1% relative humidity, and the maximum mean deviations over a 10-min period with constant setpoints were $2.5 \text{ }^\circ\text{C}$ air temperature and 5% relative humidity.

© 2011 IAGrE. Published by Elsevier Ltd. All rights reserved.

1. Introduction

The high capital investment associated with a greenhouse must be justified by its ability to provide year-round high quality produce. In warm regions, such as the Mediterranean area, the hot weather severely limits greenhouse production during a significant part of the year (usually from late May to September). During these months, greenhouses are either not in use or generate low quality produce. In the current global

and highly competitive market, the inability to deliver high quality produce year-round makes it impossible for the growers to secure long-term markets, which may have disastrous consequences. Extending the production period of greenhouse through the hot summer months is therefore a priority in such regions.

During periods of high heat load (high solar radiation and air temperature), ventilation alone is not always capable of removing a sufficient amount of the energy that enters the

* Corresponding author. Tel.: +972 4 8295902; fax: +972 4 8228898.

E-mail address: linkerr@tx.technion.ac.il (R. Linker).

1537-5110/\$ – see front matter © 2011 IAGrE. Published by Elsevier Ltd. All rights reserved.

doi:10.1016/j.biosystemseng.2011.07.010

threshold levels (“thermostatic control”) is theoretically possible, such simplistic control is not only highly inefficient but also very risky since excessive fogging may result in water deposition on the canopy, with the associated risk of damage to the plants. In addition, it must be noted that when fogging is used, increasing the ventilation rate does not necessarily lead to a decrease of the air dry-bulb temperature (Arbel et al., 2003). Such non-intuitive behaviour of the system further stresses the need for advanced automatic control.

The development of control strategies for fogging systems in greenhouses has been investigated by Arbel et al. (1999, 2003), Handarto et al. (2006) and Sase et al. (2006). These studies were based on a static description of the greenhouse and the crop, and resulted in “if-then” control rules. Haeussermann et al. (2007) who investigated the use of a fogging system in pig-houses also relied on simple thermostatic “if-then” control rules. Such an approach fails to consider two important characteristics of greenhouses. Firstly, such systems are dynamic by nature and a static representation is overly simplistic. Secondly, the simple mathematical models that are used to describe the greenhouse climate and determine the control rules are not perfect. More specifically, most of the parameters that are included in the models are known only approximately, either because they cannot be measured directly or because during the parameter identification procedure unmodelled processes are reflected through variation of the parameters. In control terminology, such systems are called “uncertain”. In order to ensure adequate performance, such systems should be controlled using either adaptive or robust controllers (e.g. Skogestad & Postlethwaite, 2005). Such a robust controller for temperature and humidity in animal buildings was developed by Soldatos, Arvanitis, Daskalov, Pasgianos, and Sigrimis (2005) and Daskalov, Arvanitis, Pasgianos, and Sigrimis (2006), extending the work of Pasgianos, Arvanitis, Polycarpou, and Sigrimis (2003) who developed a controller based on a dynamic model that did not take parameter uncertainties into account. The present work investigates an alternative approach and focuses on the design of a robust linear time invariant controller for greenhouse temperature and humidity, using the quantitative feedback theory (QFT) loop-shaping technique (Horowitz, 1991; Horowitz & Sidi, 1972). This approach was chosen since it offers a highly transparent design process and typically yields simple low order controllers that can be easily implemented. In addition, QFT is a natural extension of classical Bode loop-shaping and is easy to grasp for anyone familiar with the Nichols chart. Various QFT software, ranging from stand-alone applications to third-party toolbox codes for Matlab, is currently available.

2. Greenhouse description

This study was conducted in a single-span glass-covered 18 m × 6 m experimental greenhouse located at the Agricultural Research Organization Center, Bet-Dagan, Israel. Dry-bulb and wet-bulb temperatures were measured at a height of 0.5 m at the centre of the greenhouse using thermocouples (type T) housed in an aspirated and shielded enclosure. Similar thermocouples were used to measure the outdoor dry-

bulb and wet-bulb temperatures. A pyranometer (LI-200, LI-COR Inc., Lincoln, NE, USA) was used to measure the incoming shortwave solar radiation at a height of 6 m above the greenhouse. All sensors were connected to a data acquisition module (FieldPoint2000, National Instruments, Austin, TX, USA) interfaced with a custom LabView (National Instruments, Austin, TX, USA) application that controlled the greenhouse operation with a sampling period of 10 s. The ventilation system consisted of six air-extracting 0.41 m fans (E404M, Vortice Corp., Burton in Trent, UK), located in the bottom part of the side walls of the greenhouse. Openings along the greenhouse roof axis were kept opened at an angle of 15° throughout the study. The greenhouse was equipped with two high-pressure fogging lines with a total of 23 nozzles (nominal flow 4 l h⁻¹ at 7 MPa), running at gutter height near the greenhouse axis. The pressure in the fogging lines could be varied continuously from 0 to 10 MPa using a variable-speed pump (A. R. Inc., Fridley, MN, USA; 8 l min⁻¹ at 14 MPa, operated by a 1.1 kW motor). The fans and the pump were controlled by the LabView application via FieldPoint2000 output modules and appropriate drivers. No plants were present in the greenhouse but the greenhouse floor was covered with lawn carpets to aerodynamically mimic a mature transpiring crop.

3. System modelling and control approach

For control purposes, greenhouse air is most conveniently described using the enthalpy and humidity ratio, which can be both described adequately by first order differential equations. For the enthalpy, the equation reads:

$$\rho l \frac{dh_i}{dt} = \alpha I - \rho C_p q (T_i - T_o) - \rho \lambda q (w_i - w_o) - U(T_i - T_o) \quad (1)$$

where h_i is the enthalpy of the greenhouse air, T_i , T_o , w_i and w_o denote the indoor and outdoor temperature and humidity ratio, respectively, q is the air exchange rate, U is the overall heat transfer coefficient, I is the incoming shortwave solar radiation outside the greenhouse, ρ is the density of dry air, l is the mean height of the greenhouse, C_p is the specific heat of air, λ is the heat of vaporisation of water and α denotes the fraction of solar radiation that is converted into sensible and latent heat of the air inside the greenhouse. Hence, the first term in Eq. (1) describes the heat load from solar radiation, the second and third terms describe the sensible and latent heat that leave the greenhouse through ventilation, and the last term corresponds to the heat loss due to cover convection. Using the definition of enthalpy ($h = C_p T + \lambda w$), Eq. (1) can be rewritten as:

$$\rho l \frac{dh_i}{dt} = \alpha I - \rho q (h_i - h_o) - \frac{U}{C_p} (h_i - h_o) + \frac{U \lambda}{C_p} (w_i - w_o) \quad (2)$$

The equation that describes the humidity ratio is

$$\rho l \frac{dw_i}{dt} = f + e - \rho q (w_i - w_o) \quad (3)$$

where f and e denote the contributions of the fogging system and the crop, respectively, and the last term denotes the water that leaves the greenhouse due to ventilation. Models of various complexities have been developed for describing the

crop evapotranspiration (e.g. Boulard & Wang, 2000; Prenger, Fynn, & Hansen, 2002; Stanghellini & de Jong, 1995). In the present control approach, crop evapotranspiration is treated as an unmeasured disturbance, for which an accurate model is not required. Hence, the simplest possible model was adopted, which assumes that evapotranspiration is directly proportional to solar radiation:

$$e = \beta I \tag{4}$$

It is important to emphasise that this model was required only in order to perform time-domain simulations of the controlled greenhouse for validating the controllers (Section 5) and this assumption did not influence the design of the controllers.

It must be noted that Eq. (2) contains only one of the control variables, namely the ventilation rate. In other words, the effect of fogging on the air enthalpy is only indirect via the humidity ratio (i.e. last term in Eq. (2)). Furthermore, under normal operating conditions this term is about one order of magnitude smaller than the term related to the ventilation. Therefore, this term can be treated as a disturbance for the purpose of designing the controllers and the system defined by Eqs. (2) and (3) can be conveniently rewritten as:

$$\rho l \frac{dh_i}{dt} = -\rho q(h_i - h_o) - \frac{U}{C_p}(h_i - h_o) + \text{disturbances} \tag{5}$$

$$\rho l \frac{dw_i}{dt} = f - \rho q(w_i - w_o) + \text{disturbances} \tag{6}$$

Eqs. (5) and (6) describe a partially decoupled system rather than full 2-by-2 multiple input-multiple output (MIMO) system. Such a system can be controlled using a cascaded approach similar to the one used by Linker, Gutman, and Seginer (1999), and in which the ventilation is used to adjust the enthalpy while fogging is used to maintain the desired humidity ratio (Fig. 1). As indicated in the figure, this does mean that the user is required to prescribe the greenhouse climate in those terms and a user-interface converting commonly-used temperature and relative humidity setpoints into the equivalent enthalpy and humidity ratio using psychrometric relationships (Albright, 1990) can easily be added. In practice, the actual ventilation rate will differ from the prescribed one due to disturbances and imperfect modelling of the air exchange rate, so that the fog controller must assume that the ventilation rate is only approximately known. Furthermore, Eqs. 5 and (6) cannot be expected to describe exactly the greenhouse climate, so that a so-called “robust control” approach must be used (Section 5).

4. System identification

4.1. Calibration of the actuators

The fogging system was calibrated by operating the pump at various constant pressure levels while measuring directly the pressure in the pipe and the discharge of random nozzles along the pipeline. The results are shown in Figs. 2 and 3.

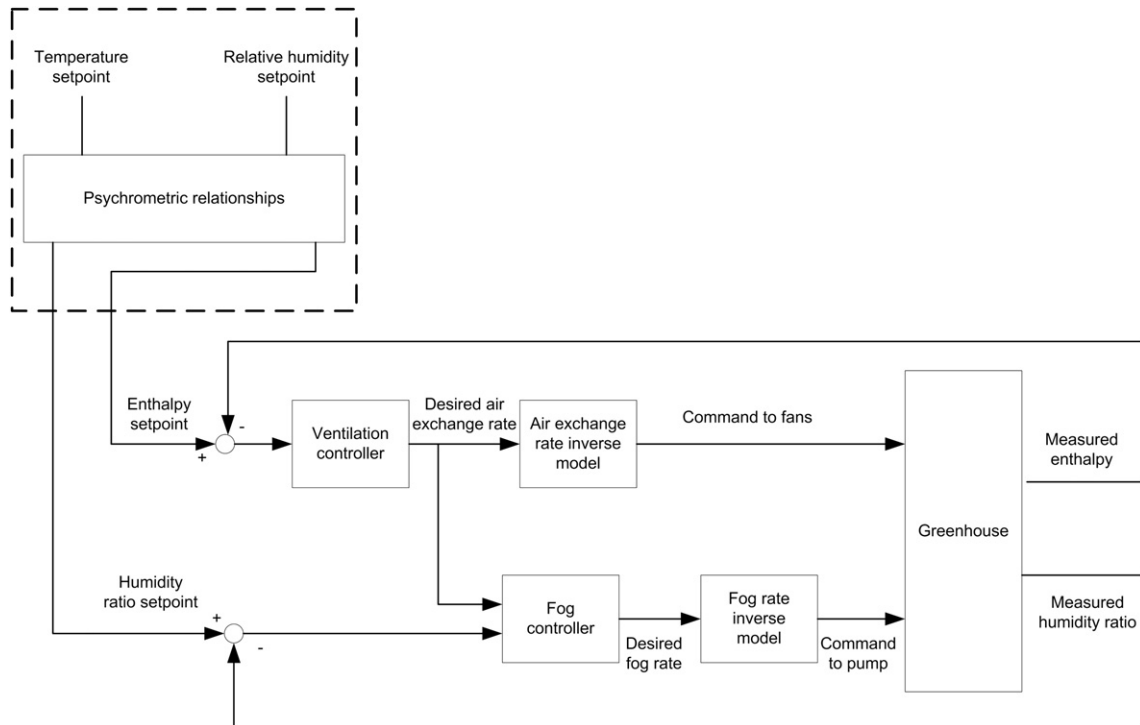


Fig. 1 – Schematic representation of the cascaded approach in which the air exchange rate is used to control the enthalpy and the fogging rate is used to control the humidity ratio, assuming the air exchange rate approximately known. The conversion included in the dashed block is optional and is required only in order to allow the grower to define the climate setpoints in terms of commonly-used variables.

Based on these results the following inverse relationships were obtained to translate the fogging rate prescribed by the controller to the command to the pump (taking into account that the nozzle pipeline includes 23 nozzles):

$$p^{\text{presc}} = 0.011 \frac{f^{\text{presc}}}{23} + 0.003 \quad (7)$$

$$S_{\text{pump}}^{\text{presc}} = -55.638(p^{\text{presc}})^2 + 2.110p^{\text{presc}} - 0.006 \quad (8)$$

The airflow of the exhaust fan was estimated in a previous study using hot-wire measurements, which led to the following relation between the current supplied to the frequency drive of the fan and the airflow through the fan (unpublished results):

$$v = -1709.8 S_{\text{fan}}^2 + 104.4 S_{\text{fan}} - 2.3 \quad (9)$$

where S_{fan} is the fan control signal and v is the resulting airflow. In order to take into account the fact that some air exchange through the roof openings occurs when the fans are turned off, the actual ventilation rate, q , was modelled as

$$q = \frac{6}{108} v + \phi, \quad (10)$$

where the first factor was introduced to account for the six fans and the greenhouse floor surface. The “leakage” air exchange (ϕ) was estimated experimentally as described in the next section.

4.2. Calibration of the enthalpy and humidity models

In order to estimate the four parameters (U , ϕ , α , β) that appear in Eqs. (2), (3) and (10) the greenhouse was operated without fogging and with the following ventilation sequences: fans at full power for 30 min, fans turned off for 10 min and fans operated at a constant but arbitrary level for 20 min. Typical results are shown in Figs. 4 and 5. These experiments showed that a pure time delay exists between the fan operation and

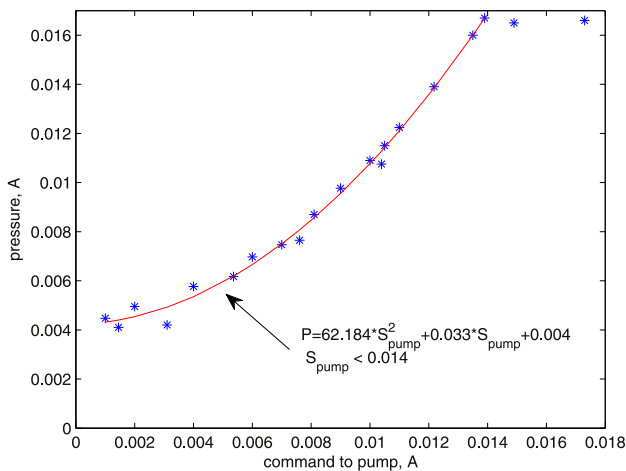


Fig. 2 – Relationship between the control signal sent to the frequency drive of the pump motor (current S_{pump}) and the pressure measured in the pipe. The * symbols correspond to measurements and the solid curve shows the fitted model.

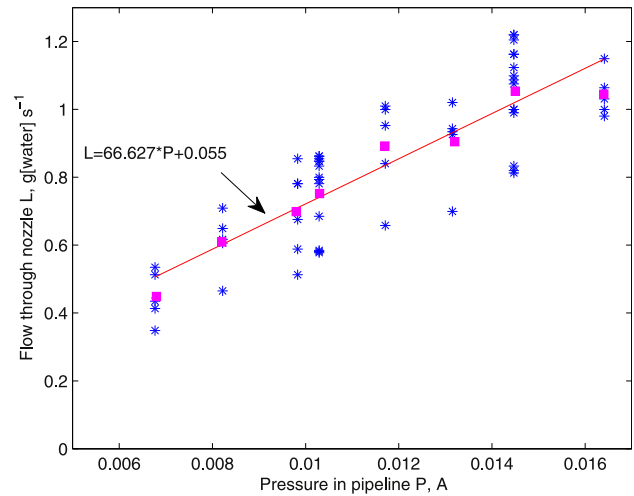


Fig. 3 – Relationship between the pressure measured in the pipe and nozzles flow rate. The * symbols correspond to measurements and the ■ symbols correspond to the average of the measurements at each pressure. The solid line shows the fitted model.

the response of the enthalpy and humidity ratio (see inserts in the Figures). Therefore, the models defined by Eqs. (2), (3) and (10) were modified to include this delay of τ s:

$$\rho l \frac{dh_i(t)}{dt} = -\rho q(t-\tau) \cdot (h_i(t-\tau) - h_o(t-\tau)) - \frac{U}{C_p} (h_i(t) - h_o(t)) + \alpha I(t) + \frac{U \cdot \lambda}{C_p} (w_i(t) - w_o(t)) \quad (11)$$

$$\rho l \frac{dw_i(t)}{dt} = f(t) - \rho q(t-\tau) (w_i(t-\tau) - w_o(t-\tau)) + \beta I(t) \quad (12)$$

Each 60-min sequence was analysed separately and the [U , ϕ , α , β , τ] combination that produced the best fit between the estimated and measured values was recorded. As can be seen in Figs. 4 and 5, after fitting the parameters, Eqs. (11) and (12) predicted well the enthalpy and the humidity ratio. Combining the results of all the sequences led to the following uncertain intervals for the parameters:

$$\begin{aligned} \phi &= [0.02 - 0.03] \\ U &= [7 - 11] \\ \alpha &= [0.3 - 0.7] \\ \beta &= [25 \times 10^{-6} - 100 \times 10^{-6}] \\ \tau &= [20 - 40] \end{aligned} \quad (13)$$

It is noteworthy to mention that, the values of α , β and ϕ were not required for designing the controllers since these parameters are associated only with disturbances (See the Eqs. (15) and (23) below).

5. Design of the controllers

The controllers were designed using QFT method, which is a loop-shaping procedure in which the user designs a feedback controller and a pre-filter in an interactive fashion. The feedback controller is most conveniently designed in a Nichols

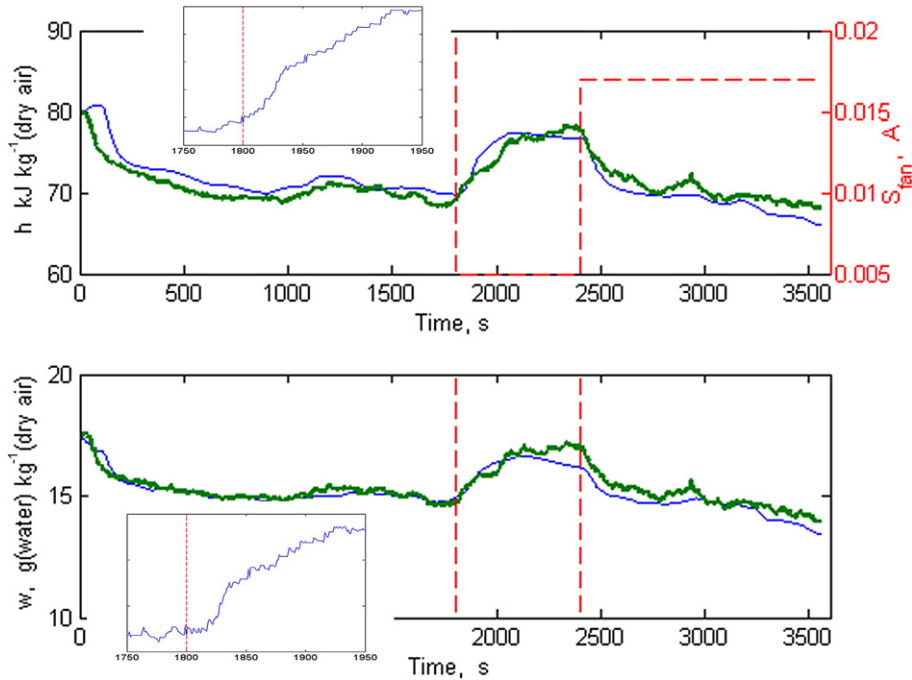


Fig. 4 – Top frame: Command to fans (red dashed line, right Y-axis) and measured (thin blue line) and predicted (bold green line) enthalpy vs. time. Bottom frame: Measured (thin blue line) and predicted (bold green line) humidity ratio vs. time. The inserts show in more details the response of the system to the fans switch-off at time 1800 s. The outside enthalpy, humidity ratio and solar radiation remained within 59–66 kJ g^{-1} , 12–14 g kg^{-1} and 740–880 W m^{-2} during the period shown.

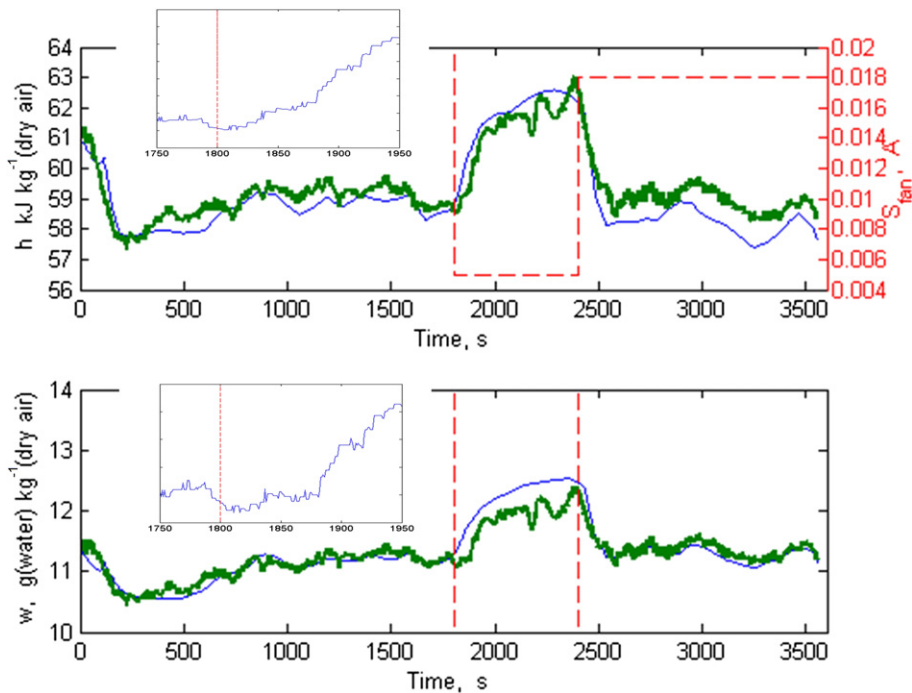


Fig. 5 – Top frame: Command to fans (red dashed line, right ordinate) and measured (thin blue line) and predicted (bold green line) enthalpy vs. time. Bottom frame: Measured (thin blue line) and predicted (bold green line) humidity ratio vs. time. The inserts show in more details the response of the system to the fans switch-off at time 1800 s. The outside enthalpy, humidity ratio and solar radiation remained within 54–57 kJ g^{-1} , 9.5–11 g kg^{-1} and 300–500 W m^{-2} during the period shown.

chart. The procedure starts with the choice of a nominal model and the computation of the value-sets (also called templates) that describe the uncertainty of the model at selected frequencies. These value-sets are then combined with the design specifications to yield a series of bounds that the nominal open-loop (feedback controller and nominal system) has to respect in order for the closed-loop system to be stable and meet the specifications. The design procedure ends with the design of a pre-filter. A detailed description of the method can be found in the papers of Horowitz and Sidi (1972) and Horowitz (1991) or in various textbooks such as by Houpis, Rasmussen, and Garcia-Sanz (2006).

5.1. Enthalpy control loop

The QFT approach selected in this work requires linearization of the model for designing the controller. Since the outdoor conditions change slowly, introducing $\theta = h_i - h_o$ and neglecting the outdoor variations altogether, Eq. (11) yields:

$$\rho l \frac{d\theta(t)}{dt} = -\rho q(t - \tau)\theta(t - \tau) - \frac{U}{C_p}\theta(t) + \alpha I(t) \tag{14}$$

Since the inside and outside enthalpies are being measured and change slowly, feedback linearisation can be used to linearise the bi-linear Eq. (14) (Gutman, 1981). Introducing the new control variable $\psi = q \cdot \theta$ and applying the Laplace transform yields the transfer function:

$$\frac{\Theta}{\Psi} = \frac{-\rho e^{-\tau s}}{\rho l s + \frac{U}{C_p}} \tag{15}$$

As a final step before designing the controller, it is necessary to include an additional uncertain gain in the model that reflects the fact that the actual ventilation rate is not equal to the desired one. Since the accuracy of the ventilation model Eq. (10) and the influence of the wind on the air exchange rate could not be estimated rigorously, an uncertainty of $\pm 25\%$, which is probably overly conservative, was considered, leading to the final design model:

$$\Omega_h = \frac{\Theta}{\Psi} = \frac{-\eta \rho e^{-\tau s}}{\rho l s + \frac{U}{C_p}} \tag{16}$$

where the three uncertain parameters are $\eta = [0.75-1.25]$, $U = [7-11]$ and $\tau = [20-40]$. The QFT design procedure requires that the user defines a nominal value for each parameter. However, these nominal values can be chosen arbitrarily (within the uncertainty range of the respective parameter) and their actual values do not affect the subsequent results. The following values were used: $\eta = 1$, $U = 9$ and $\tau = 30$.

The following specifications were chosen for the controlled loop:

- Zero steady-state error in response to step change in reference signal
- Maximum overshoot: 15%
- Rise time (90%): 150–420 s
- Convergence time ($\pm 10\%$): 480 s
- $1/1 + G_h \cdot \Omega_h \leq 6$ dB, where G_h denotes the feedback controller

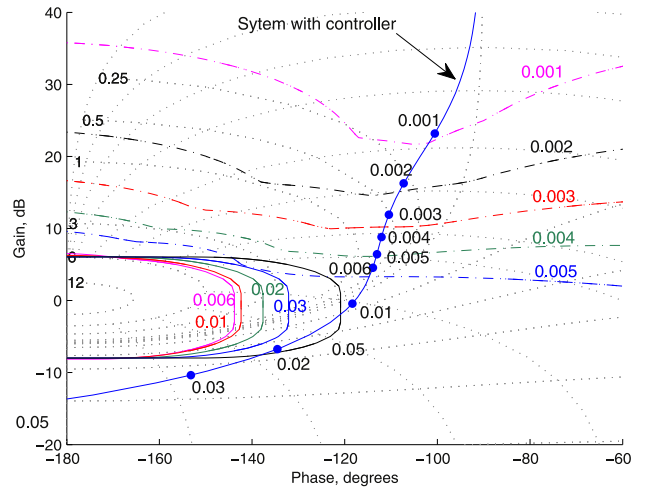


Fig. 6 – Nichols chart (gain vs. phase) showing the frequency function of the nominal open-loop model (Eq. (16) with nominal parameter values and the controller (17)), together with Horowitz–Sidi bounds. The dash-dot lines correspond to the tolerance bounds and the solid lines to the sensitivity bounds.

The last specification guarantees closed-loop stability and implies a worst-case gain margin and phase margin of approximately 6 dB and 30°, respectively. Although the time-domain specifications may seem lenient, their choice was dictated by the large delay and gain uncertainty that exist in the model, and by the fact that under normal operation the setpoint is not expected to change abruptly. Following the QFT procedure as implemented in the design software Qsyn

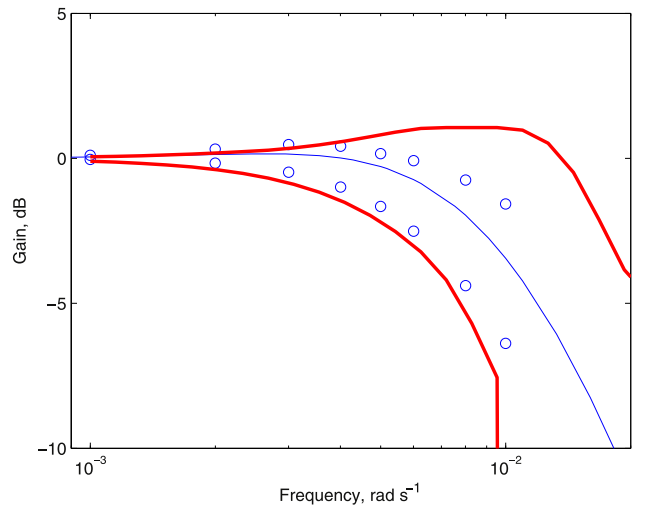


Fig. 7 – Gain of compensated closed-loop with pre-filter ($F_h \cdot G_h \cdot \Omega_h / (1 + G_h \cdot \Omega_h)$). The bold lines denote the range in which the closed-loop must be in order to meet design specifications. The solid line represents the nominal system and the circles show the range of the closed-loop gain at the frequencies at which the value-sets were computed.

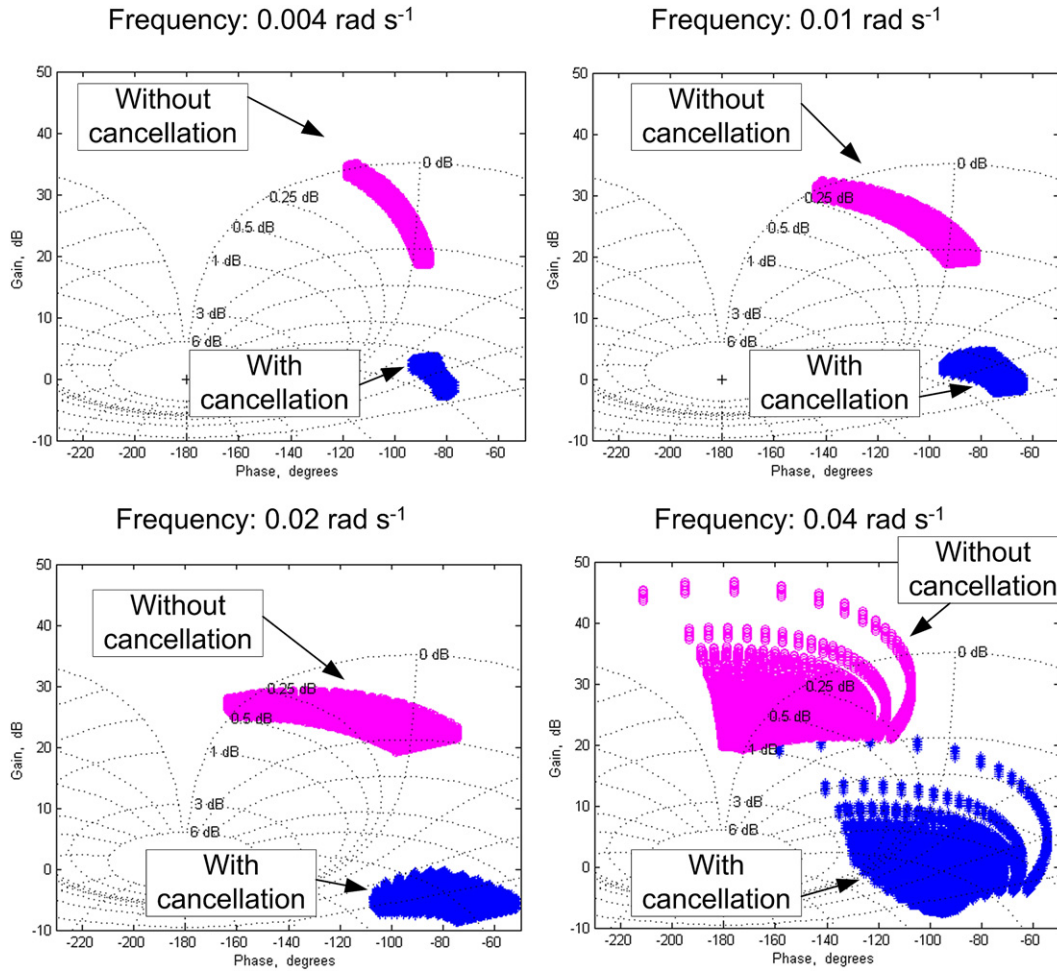


Fig. 8 – Nichols chart showing the value-sets of Eq. (23) (no cancellation of the nominal system) and Eq. (24) (with cancellation of the nominal system) at four frequencies. Since only the extent of each value-set is of importance, some of the value-sets were shifted in order to avoid overlapping and to enhance clarity.

(Gutman, 1996), the time-domain specifications were translated to frequency domain specifications assuming that the resulting closed-loop would behave as a second order system. These specifications, together with the value-sets of the model (Eq. (16)), were used to compute the Horowitz–Sidi bounds shown in Fig. 6. The sensitivity bounds (shown for selected frequencies as solid lines around the instability point $(-1 + 0 \cdot j)$) correspond to the location of the nominal open-loop closest to the instability point $(-1 + 0 \cdot j)$ for which the specification $1/(1 + G_h \cdot Q_h) \leq 6$ dB is met at the respective frequency. In order for the closed-loop to be stable, the nominal open-loop at each frequency must be outside the sensitivity bound of the corresponding frequency. The tolerance bounds (shown for selected frequencies as dot-dashed lines in Fig. 6) correspond to location of the nominal open-loop that ensures that the closed-loop system meets the frequency domain specifications. In order to meet the specifications, the nominal open-loop at each frequency must be above the corresponding tolerance bound. A suitable controller is found by iterative trial-and-error loop shaping during which the designer modifies the form and the parameters of the controller until the design specifications are met.

This procedure led to adoption of the following simple PI (proportional-integral) feedback controller:

$$G_h(s) = 25 \times 10^{-3} \cdot \frac{s + 4 \times 10^{-3}}{s} \cdot \frac{1 - e^{-10 \cdot s}}{10 \cdot s} \quad (17)$$

where the last factor corresponds to the sample-and-hold operation that will be embedded in the discrete controller (Franklin, Powell, & Workman, 1998). Fig. 6 shows that the closed-loop with this controller meets the specifications. Although a tighter design could be achieved, some safety margin relative to the sensitivity bounds was kept in order to account for some phase loss when discretising the controller.

The following low-pass pre-filter was added to adjust the system bandwidth according to the specifications:

$$F_h(s) = \frac{0.01}{s + 0.01} \quad (18)$$

and Fig. 7 shows that the compensated closed loop $F_h G_h Q_h / (1 + G_h Q_h)$ fulfils the design specifications.

For implementation, $G_h(s)$ and $F_h(s)$ were translated to their respective discrete forms using the matched zero-pole method (Franklin et al., 1998):

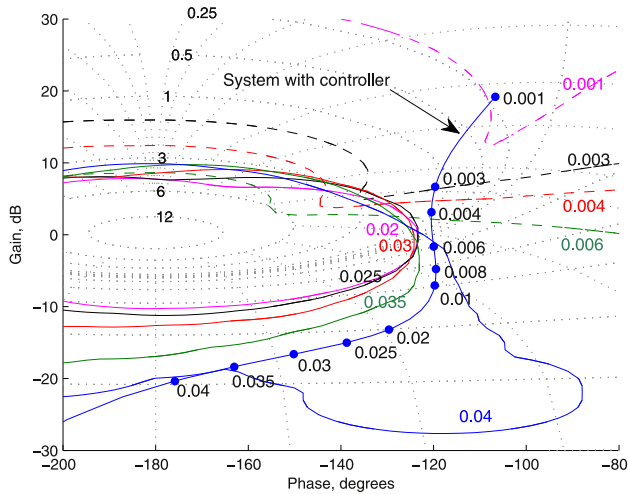


Fig. 9 – Nichols chart showing the frequency function of the nominal open-loop (model Eq. (24) with nominal parameter values and the controller Eq. (25)), together with Horowitz–Sidi bounds. Symbols as in Fig. 6.

$$G_h(z) = \frac{-25.5 \times 10^{-3} z + 24.5 \times 10^{-3}}{z - 1} \quad (19)$$

$$F_h(z) = 47.6 \times 10^{-3} \frac{z + 1}{z - 0.9048} \quad (20)$$

Rechecking the loop-shaping design with $G_z(s)$ showed that the closed-loop was stable and met the design requirements (not shown).

5.2. Humidity ratio control loop

Introducing $v = w_i - w_o$ and assuming slow variations of the outdoor humidity ratio, Eq. (12) can be rewritten as

$$\rho \cdot l \frac{dw(t)}{dt} = f(t) - \rho q(t - \tau) v(t - \tau) + \beta I(t) \quad (21)$$

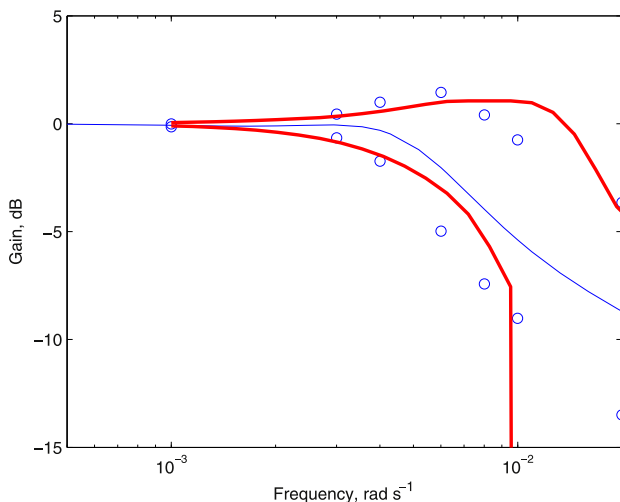


Fig. 10 – Gain of compensated closed-loop ($F_h \cdot G_w \cdot \Omega_w / (1 + G_w \cdot \Omega_w)$). Symbols as in Fig. 7.

which yields the following transfer function between the fogging rate and the humidity ratio:

$$\Omega_w = \frac{Y}{F} = \frac{\kappa}{\rho \cdot l \cdot s + \rho \cdot Q \cdot e^{-\tau \cdot s}} \quad (22)$$

where κ is an additional uncertain parameter that takes into account the fact that the fogging rate realised in the greenhouse will not be the prescribed one. This uncertainty can be estimated from Figs. 2 and 3 that show the relations that were found between the control signal sent to the variable-speed pump, the water pressure and the nozzles' flow rate. Based on these results, the uncertainty range of κ was set to (0.9–1.1).

Following the cascade approach, the ventilation rate may be assumed to be known approximately ($Q = \eta \cdot Q^{presc}$), which yields:

$$\Omega_w = \frac{Y}{F} = \frac{\kappa}{\rho \cdot l \cdot s + \rho \cdot \eta \cdot Q^{presc} \cdot e^{-\tau \cdot s}} \quad (23)$$

where Q^{presc} is treated as an uncertain parameter with range (0.02–0.07). The value-sets of this system at selected frequencies are shown in Fig. 8. The area defined by each value-set contains all the feasible values of the uncertain transfer function Eq. (23) at the corresponding frequency, i.e. it represents the model uncertainty. Since the main purpose of the feedback controller is to ensure that the uncertainty that remains after closing the loop is sufficiently small (so that the system's response is within the specifications), the larger the value-set, the harder the task of designing the controller. In the present case, the uncertainty that has to be handled by the feedback controller can be reduced by including in the controller an inverse model of the system (Linker et al., 1999) so that the system for which the controller has to be designed is:

$$\Omega_w = \frac{\kappa \cdot (\rho \cdot l \cdot s + \rho \cdot Q^{presc})}{\rho \cdot l \cdot s + \rho \cdot \eta \cdot Q^{presc} \cdot e^{-\tau \cdot s}} \quad (24)$$

The advantage of using such a partial cancellation can be appreciated by comparing the value-sets of the original system Eq. (23) with those of the transfer function Eq. (24) obtained after partial cancellation (Fig. 8). Clearly, including in the controller the inverse nominal model of the system reduces the uncertainty that has to be handled by the feedback controller, especially at low frequencies.

The specifications chosen for the closed-loop were similar to the ones used for the enthalpy, which yielded the Sidi–Horowitz bounds shown in Fig. 9. The most problematic bound is the sensitivity (stability) bound at $4 \times 10^{-2} \text{ rad s}^{-1}$, which severely restricts the achievable closed-loop performance. Trial-and-error loop shaping led to the following feedback controller:

$$G_w(s) = 8 \cdot 10^{-5} \cdot \frac{1}{s} \cdot \frac{s + 5 \cdot 10^{-3}}{s + 2 \cdot 10^{-3}} \cdot \frac{1}{s + 0.02} \cdot \frac{1 - e^{-10 \cdot s}}{10 \cdot s} \quad (25)$$

in which the last factor corresponds to the sample-and-hold operation that will be embedded in the discrete controller. Fig. 9 shows that the closed-loop with this controller meets the specifications, except at frequencies around $4 \times 10^{-3} - 6 \times 10^{-3} \text{ rad s}^{-1}$ where the nominal loop is slightly below the corresponding tolerance bound. However, the violation is minimal and does not jeopardise the overall

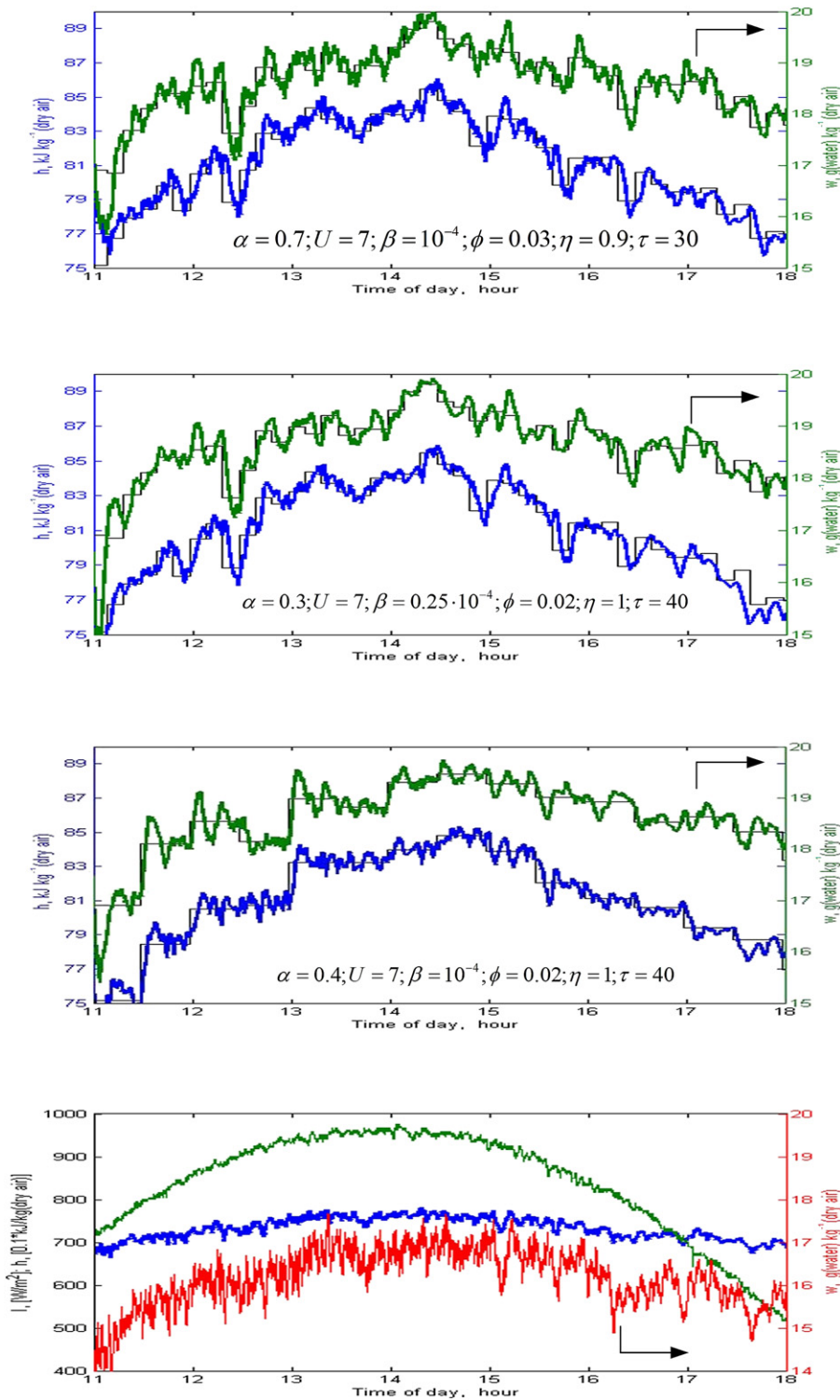


Fig. 11 – Results (scaled enthalpy on left ordinate; humidity ratio on right ordinate) of simulations based on the models Eqs. (2) & (3) with the controllers and pre-filter Eqs. (19), (20), (27) and (28). The setpoints ($h_{set} = h_o + 8000$; $w_{set} = w_o + 2.5$ adjusted every 10 min in the two top simulations and every 30 min in the third simulation) are shown by the thin lines and the simulated responses are shown in bold. The values of the parameters are indicated in each frame. The bottom frame shows the weather used (July 7, 2010) – solar radiation and scaled enthalpy (left ordinate) and humidity ratio (right ordinate).

Table 1 – Summary of the tracking performance (simulations based on Eqs. (2) and (3)) for ten combinations of the parameters. The first three combinations are the same as in Fig. 11. The weather and setpoints in all simulations are the ones shown in Fig. 11.

Combination number	Parameters						Enthalpy, J kg ⁻¹ [dry air]		Humidity ratio, g [water] kg ⁻¹ [dry air]	
	α	U	β	ϕ	η	τ	mean ($h_{set}-h_i$)	std ($h_{set}-h_i$)	mean ($w_{set}-w_i$)	std ($w_{set}-w_i$)
1	0.70	7	1·10 ⁻⁴	0.030	0.9	30	91	1029	0.046	0.354
2	0.30	7	2.5·10 ⁻⁵	0.020	1.0	40	175	1070	0.025	0.368
3	0.40	7	1·10 ⁻⁴	0.020	1.0	40	79	1041	0.025	0.358
4	0.40	7	1·10 ⁻⁴	0.020	1.0	30	76	996	0.025	0.351
5	0.50	10	5·10 ⁻⁵	0.025	1.1	30	67	941	0.026	0.350
6	0.50	10	5·10 ⁻⁵	0.025	0.9	60	57	1094	0.028	0.374
7	0.60	11	7.5·10 ⁻⁵	0.025	0.9	50	51	1060	0.030	0.361
8	0.35	8	3.5·10 ⁻⁵	0.030	0.9	35	295	1028	0.023	0.371
9	0.35	8	2.5·10 ⁻⁵	0.030	0.9	55	299	1080	0.025	0.377
10	0.55	9	6·10 ⁻⁵	0.025	1.1	45	63	1015	0.028	0.352

performance of the closed-loop. Such small violation is highly preferable to the alternative; a much tighter design that brings the loop dangerously close to some of the sensitivity bounds.

Fig. 10 shows that after the addition of the pre-filter

$$F_w(s) = 2.143 \cdot \frac{s + 4 \times 10^{-3}}{s + 2.5 \times 10^{-3}} \cdot \frac{s + 7 \times 10^{-3}}{s + 24 \times 10^{-3}} \quad (26)$$

the compensated closed loop $F_w \cdot G_w \cdot \Omega_w / (1 + G_w \cdot \Omega_w)$ is close to fulfilling the design specifications. At this point, the fact that some of the frequency-domain design specifications are not met is not a major concern since the final appraisal of the controller performance must be performed in the time-domain (Section 6).

The equivalent discrete-form of the controller obtained using the matched zero-pole method, is:

$$G_w(z) = 1.1 \times 10^{-3} \cdot \frac{z + 1}{z - 1} \cdot \frac{1.015 \cdot z - 0.966}{z - 0.9802} \cdot \left[3.956 \cdot \frac{Q^{presc}}{1 - e^{-4.364 \cdot Q^{presc}}} \cdot \frac{z - e^{-4.364 \cdot Q^{presc}}}{z - 0.819} \right] \quad (27)$$

in which the term in brackets corresponds to the inverse model and the pole at $s = 0.02$. Rechecking the loop-shaping design with $G_w(z)$ showed that the closed-loop was stable.

The equivalent discrete-form of the pre-filter is:

$$F_w(s) = \frac{2.159 \cdot z - 2.074}{z - 0.9753} \cdot \frac{0.9205 \cdot z - 0.8583}{z - 0.7866} \quad (28)$$

6. Results

6.1. Simulation results

The controllers were initially validated by numerical simulations based on the non-linear model described by Eqs. (2) and (3), and typical results corresponding to three combinations of the uncertain parameters are shown in Fig. 11. For simplicity, in these simulations, the enthalpy and humidity ratio setpoints were calculated as $h_{set} = (h_o + 8000)$ and $w_{set} = (w_o + 2.5)$. It can be seen that the setpoints were tracked in a satisfactory fashion regardless of the values of the uncertain parameters. A quantitative analysis of the controllers' performance is shown in Table 1 which presents the mean and standard

deviation of the tracking errors of both variables, when the setpoints are adjusted every 10 min. These results correspond to the three parameter combinations shown in Fig. 11 and seven additional combinations. For all ten combinations, the humidity setpoint is tracked very accurately with a mean error of less than 0.050 g [water] kg⁻¹ [air] (less than 0.030 g [water] kg⁻¹ [air] in nine cases) and a standard deviation of less than 0.400 g [water] kg⁻¹ [air]. For the enthalpy, the standard deviation of the tracking error is around 1000 J kg⁻¹ [dry air] in all simulations and the mean tracking error is less than 100 J kg⁻¹ [dry air] in seven cases. The three cases with a higher mean tracking error (combinations 2, 8 and 9) corresponded to very low values of the parameter α , meaning that only a small fraction of the incoming solar radiation was converted into energy in the greenhouse air. As a result, the desired setpoint cannot be maintained during part of the day, even if the fans are turned off. More specifically, the controller turned off the fans at 16:00 in simulations 8 and 9, and at 17:15 in simulation 2. The latter can be observed in Fig. 11 (second frame), in which the enthalpy is consistently below the setpoint after approximately 17:30. Clearly, in such cases the relatively large tracking error should not be blamed on the feedback controller but rather indicates that the strategy for determining the setpoints (which is beyond the scope of the present paper) should be modified to ensure the feasibility of the setpoints.

6.2. Implementation results

Implementation results are shown in Figs. 12–15. During these experiments the setpoints were calculated as simple functions of the outdoor conditions. Clearly, in practice, these setpoints could be determined in a much more complex fashion, taking into account for instance the type of crop, its growth stage, etc. However, the generation of such elaborate setpoints is a separate issue altogether which is beyond the scope of the present paper. Clearly, the way the setpoints were determined does not affect the performance of the controllers *per se*. Figs. 12 and 13 show the enthalpy and humidity ratio recorded on July 15 and July 18, 2010, respectively, during which the setpoints were at first gradually increased or decreased and then maintained at constant values for the rest of the day (except for the humidity ratio that was gradually

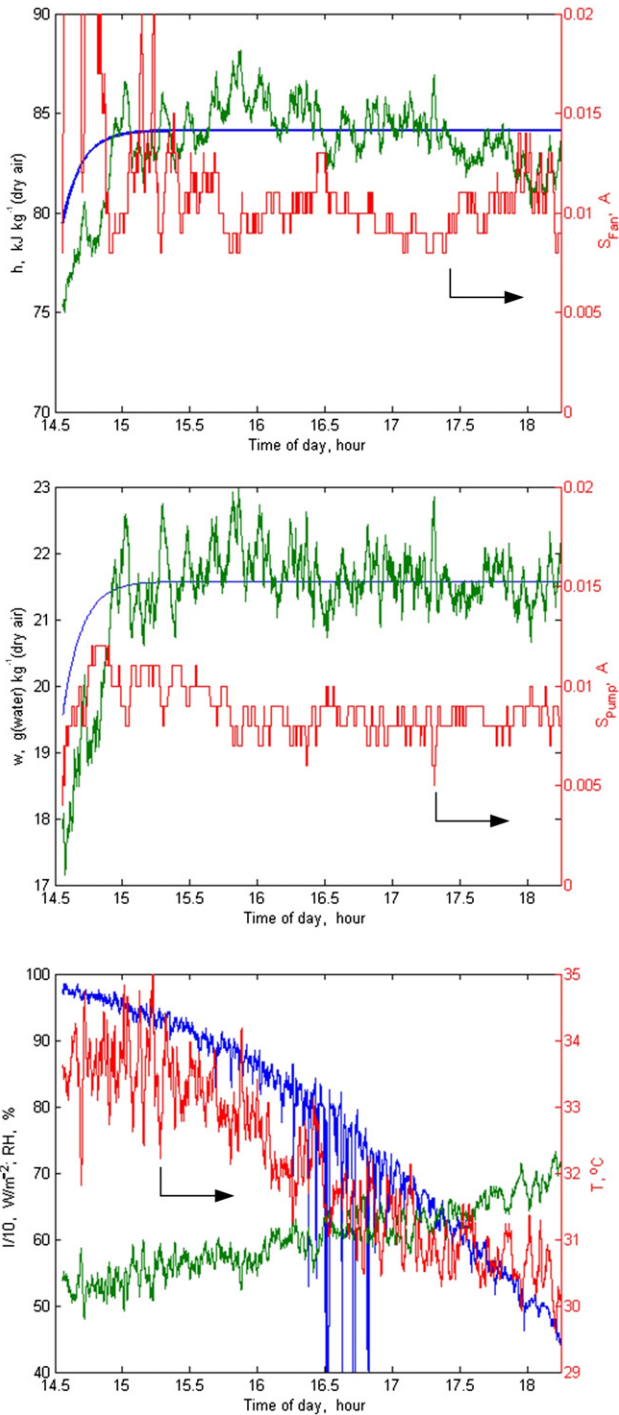


Fig. 12 – Experimental results of July 15, 2010. Top frame: Enthalpy setpoints (blue) and measurements (left ordinate) and command to fans (right ordinate). Middle frame: Humidity ratio setpoints (blue) and measurements (left ordinate) and command to pump (right ordinate). Bottom frame: Outdoor solar radiation, relative humidity (left ordinate) and temperature (right ordinate).

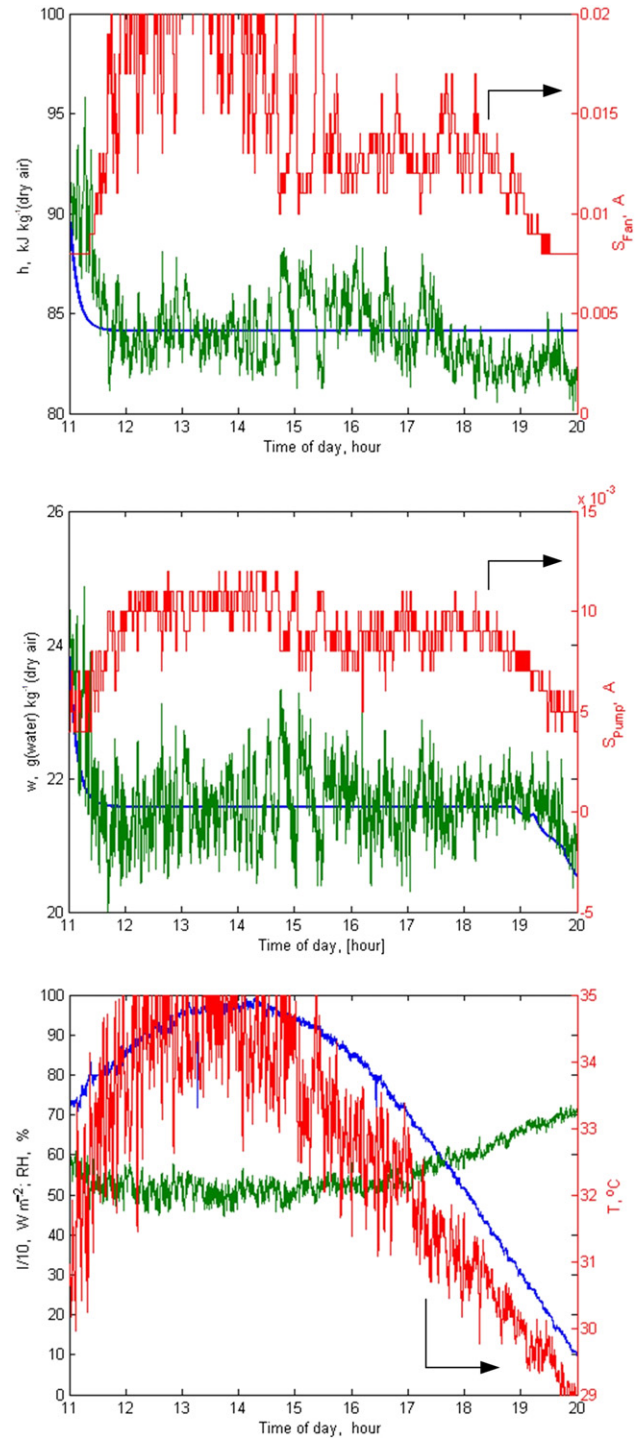


Fig. 13 – Experimental results of July 18, 2010. Frames arrangement and symbols as in Fig. 12.

lowered after 19:00 on Aug 18). These figures show that on both days the controllers brought the indoor climate close to the setpoints and maintained the desired climate inside the greenhouse despite the very large diurnal variation of the

outdoor environment (bottom frames of the Figures). Table 2 summarises the average performance of the controllers during the periods with constant setpoints. Overall, the mean tracking error for the enthalpy was around 100 J kg^{-1} [dry air], which is similar to the error achieved in most simulations. The standard deviation was higher ($\sim 1500 \text{ J kg}^{-1}$ [dry air]) compared to $\sim 1000 \text{ J kg}^{-1}$ [dry air] in the simulations), but still acceptable. For the humidity, the standard deviation is similar

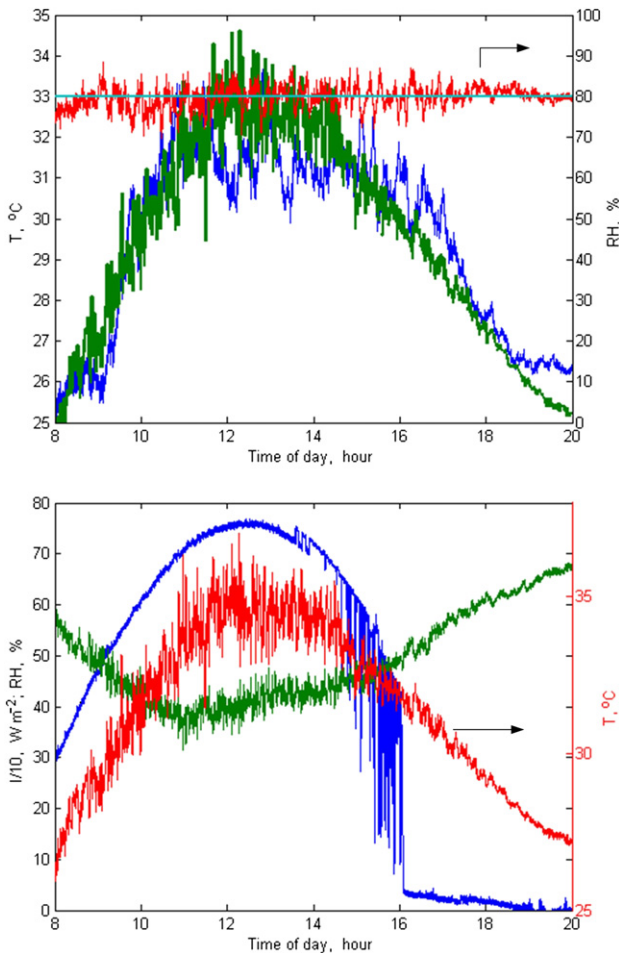


Fig. 14 – Experimental results of August 2, 2010. Top frame: Temperature setpoints (blue) and measurements (left ordinate) and relative humidity setpoints (constant, 80%) and measurements (right ordinate). Bottom frame: Outdoor solar radiation, relative humidity (left ordinate) and temperature (right ordinate). The solar radiation measurements after 16:00 are inaccurate due to sensor shading.

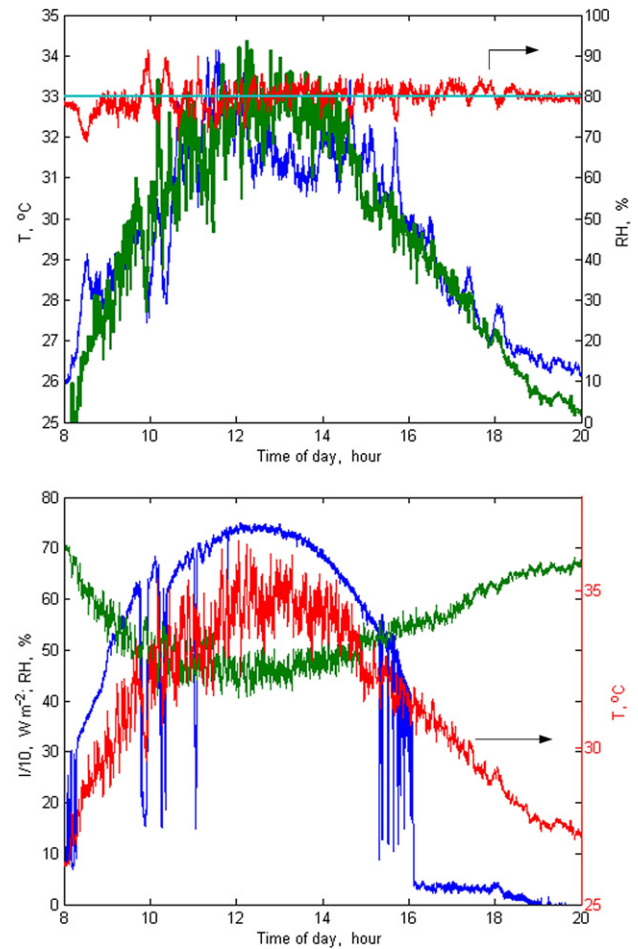


Fig. 15 – Experimental results of August 5, 2010. Frames arrangement and symbols as in Fig. 14. The solar radiation measurements after 16:00 are inaccurate due to sensor shading.

to that of the simulations ($\sim 0.4 \text{ g [water] kg}^{-1} \text{ [dry air]}$) but the mean error is significantly larger ($\sim 0.10 \text{ g [water] kg}^{-1} \text{ [dry air]}$ compared to $\sim 0.03 \text{ g [water] kg}^{-1} \text{ [dry air]}$ in simulations). The fact that the experimental tracking errors were larger than in the simulations is not surprising, especially considering that the influence of the wind was not considered at all in the models, while in practice the fog lines are located close to the roof openings and some of the droplets may be carried away before they evaporate. Still, these experimental results are entirely satisfactory and demonstrate the robustness of the developed controllers.

Since in practice, air temperature and relative humidity (or equivalently air temperature and vapour pressure deficit) are usually used by growers to describe the greenhouse climate, Figs. 14 and 15 show the results obtained on two additional days during which the setpoints were expressed using these variables. During these tests, the temperature setpoint was adjusted every 10 min based on the outside temperature while

the relative humidity setpoint remained at 80%. Although such a strategy is somewhat arbitrary, its sole purpose was to illustrate the performance of the controllers, which should be independent of the setpoints strategy as long as these setpoints are achievable. In particular, it must be emphasised that maintaining such setpoints requires adjustment of the two underlying setpoints, enthalpy and humidity ratio, which were calculated using the psychrometric

Table 2 – Summary of the tracking performance during the experiments with constant setpoints shown in Figs. 12 and 13.

Date	Period used for calculation	Enthalpy, $\text{J kg}^{-1} \text{ [dry air]}$		Humidity ratio, $\text{g [water] kg}^{-1} \text{ [dry air]}$	
		mean $(h_{set}-h_i)$	std $(h_{set}-h_i)$	mean $(w_{set}-w_i)$	std $(w_{set}-w_i)$
July 15	15:00–18:30	62	1365	0.080	0.396
July 18	11:00–19:00	133	1854	0.100	0.519

Table 3 – Summary of the tracking performance during the two days of experiments shown in Figs. 14 and 15.

Date	Period used for calculation	Temperature, °C		Relative humidity, %	
		mean ($T_{set}-T_i$)	std ($T_{set}-T_i$)	mean ($RH_{set}-RH_i$)	std ($RH_{set}-RH_i$)
Aug 2	8:00–20:00	0.03	1.10	–0.29	2.65
Aug 5	8:00–20:00	0.16	1.10	–0.20	2.81

relationships as described in Fig. 1. Figs. 14 and 15 showed that on both days the controllers maintained the indoor climate close to the setpoints. Short-term deviations that resulted from sudden clouds can be seen around 10:00 on August 4. The overall tracking performance can be further appreciated in Table 3, which shows that on a daily basis there are only negligible deviations from the setpoints in both temperature and relative humidity. On both days, the maximum average deviations during the 10-min periods with constant setpoints were 2.5 °C and 5% relative humidity, which would be acceptable for most agricultural crops.

7. Conclusions

A robust control approach for maintaining the desired climate inside a greenhouse equipped with a variable-rate high-pressure fogging system and variable-speed extracting fans has been developed and tested. The proposed control scheme relies on partial decoupling between the controlled variables, which is obtained by describing the air properties using enthalpy and humidity ratio rather than the more common temperature and relative humidity or vapour pressure deficit. As emphasised in Fig. 1 and demonstrated in the results presented in Figs. 14 and 15, this choice does not restrict the ability of the user to define the climate setpoints using these more intuitive properties.

Using a robust control method such as QFT to design the controllers ensures robustness of the controlled system, i.e. guarantees acceptable performance despite the large modelling uncertainties and strong disturbances which are inherent to greenhouses. A major advantage of the proposed control scheme is that crop transpiration is treated as an unmeasured disturbance. As a result, a crop transpiration model is not required at the design stage and is needed only to perform preliminary testing of the controllers via simulations before implementation. Although such models are available in the literature, in order to be accurate enough to be used as part of a “feedforward from disturbances” or “inverse model” module they should be recalibrated (or at least validated) on-site, which requires dedicated, time-consuming measurements. By comparison, the crop transpiration used in the present scheme does not need to be very accurate since it does not affect the controllers’ performance during implementation. Furthermore, the proposed procedure requires only the estimation of a relatively small numbers of parameters that can be relatively easily estimated from a few “step change” experiments or via direct measurements (e.g. nozzles flow rates). The most limiting requirement is that a relationship

between the operation of the fans and the ventilation rate must be available. However, the large uncertainty considered for this variable ($\pm 25\%$) shows that this model does not need to be particularly accurate and in absence of actual measurements one could rely on manufacturer data.

Acknowledgements

This research was supported by Research Grant No. IS-4122-08R from BARD, the United States-Israel Binational Agricultural Research and Development Fund.

REFERENCES

- Albright, L. (1990). *Environment control for animals and plants*. New York: American Society of Agricultural Engineers.
- Arbel, A., Barak, M., & Shklyar, A. (2003). Combination of forced ventilation and fogging systems for cooling greenhouses. *Biosystems Engineering*, 84, 45–55.
- Arbel, A., Yekutieli, O., & Barak, M. (1999). Performance of a fog system for cooling greenhouses. *Journal of Agricultural Engineering Research*, 72, 129–136.
- ASHRAE. (1972). *Handbook of Fundamentals*. New York: American Society of Agricultural Engineers.
- Boulard, T., & Wang, S. (2000). Greenhouse crop transpiration model from external climate conditions. *Acta Horticulturae*, 534, 235–244.
- Cohen, Y., Stanghill, G., & Fuchs, M. (1983). An experimental comparison of evaporative cooling in a naturally ventilated glasshouse due to wetting the outer roof and inner crop soil surfaces. *Agricultural Meteorology*, 28, 239–251.
- Daskalov, P. I., Arvanitis, K. G., Pasgianos, G. D., & Sigrimis, N. A. (2006). Non-linear adaptive temperature and humidity control in animal buildings. *Biosystems Engineering*, 93, 1–24.
- Feuermann, D., Kopel, R., Zeroni, M., Levi, S., & Gale, J. (1998). Evaluation of a liquid radiation filter greenhouse in a desert environment. *Transactions of the ASAE*, 41, 1781–1788.
- Franklin, G. F., Powell, J. D., & Workman, M. (1998). *Digital control of dynamic systems* (3rd ed.). Addison-Wesley Pub.
- Giacomelli, G., Giniger, M., Krauss, A., & Mears, D. (1985). Improving methods of greenhouse evaporative cooling. *Acta Horticulturae*, 174, 49–56.
- Gutman, P. O. (1981). Stabilizing controllers for bilinear systems. *IEEE Transactions on Automatic Control*, 26, 917–922.
- Gutman, P. O. (1996). *Qsyn—The toolbox for robust control systems design for use with MATLAB—User’s guide*. Available at <http://www.math.kth.se/optsys/forskning/forskarutbildning/5B5782/index.html>.
- Haeussermann, A., Hartung, E., Jungbluth, T., Vranken, E., Aerts, J., & Berckmans, D. (2007). Cooling effects and evaporation characteristics of fogging systems in an experimental piggery. *Biosystems Engineering*, 97, 395–405.
- Handarto, M. H., Ohyama, K., Toida, H., Goto, E., & Kozai, T. (2006). Developing control logic for a high-pressure fog cooling system operation for a naturally ventilated greenhouse. *Environmental Control in Biology*, 44, 1–9.
- Horowitz, I. M. (1991). Survey of quantitative feedback theory (QFT). *International Journal of Control*, 53, 255–291.
- Horowitz, I. M., & Sidi, M. (1972). Synthesis of feedback systems with large plant ignorance for prescribed time-domain tolerances. *International Journal of Control*, 16, 287–309.

- Houpis, C. H., Rasmussen, S. J., & Garcia-Sanz, M. (2006). *Quantitative feedback theory: Fundamentals and applications* (2nd ed.). CRC Taylor & Francis.
- Kittas, C., Bartzanas, T., & Jaffrin, A. (2003). Temperature gradients in a partially shaded large greenhouse equipped with evaporative cooling pads. *Biosystems Engineering*, 85, 217–227.
- Linker, R., Gutman, P. O., & Seginer, I. (1999). Robust controllers for simultaneous control of temperature and CO concentration in greenhouses. *Control Engineering Practice*, 7, 851–862.
- Pasgianos, G. D., Arvanitis, K. G., Polycarpou, P., & Sigrimis, N. A. (2003). A nonlinear feedback technique for greenhouse environmental control. *Computers and Electronics in Agriculture*, 40, 153–177.
- Prenger, J. J., Fynn, R. P., & Hansen, R. C. (2002). A comparison of four evapotranspiration models in a greenhouse environment. *Transactions of the ASAE*, 45, 1779–1788.
- Sabeh, N. C., Giacomelli, G. A., & Kubota, C. (2006). Water use for pad and fan evaporative cooling of a greenhouse in semi-arid climate. *Acta Horticulturae*, 719, 409–416.
- Sase, S., Ishii, M., Moriyama, H., Kubota, C., Kurata, K., Hayashi, M., et al. (2006). Effect of natural ventilation rate on relative humidity and water use for fog cooling in a semiarid greenhouse. *Acta Horticulturae*, 719, 385–392.
- Skogestad, S., & Postlethwaite, I. (2005). *Multivariable feedback control, analysis & design* (2nd ed.). John Wiley & Sons.
- Soldatos, A. G., Arvanitis, K. G., Daskalov, P. I., Pasgianos, G. D., & Sigrimis, N. A. (2005). Nonlinear robust temperature–humidity control in livestock buildings. *Computers and Electronics in Agriculture*, 49, 357–376.
- Stanghellini, C., & de Jong, T. (1995). A model of humidity and its applications in a greenhouse. *Agricultural and Forest Meteorology*, 76, 129–148.